Hindawi
International Journal of Chemical Engineering
Volume 2019, Article ID 9525783, 10 pages
https://doi.org/10.1155/2019/9525783

Research Article

Predicting CO_2 Permeation through an Enhanced Ionic Liquid Mixed Matrix Membrane (IL3M)

Dzeti F. Mohshim,[1,2] **Hilmi Mukhtar**,[3] **Binay K. Dutta**,[4] **and Zakaria Man**[3]

[1]*Petroleum Engineering Department, Universiti Teknologi Petronas, 32610 Bandar Seri Iskandar, Perak Darul Ridzuan, Malaysia*
[2]*Center of Enhanced Oil Recovery, Institute of Hydrocarbon Recovery, Universiti Teknologi Petronas, 32610 Bandar Seri Iskandar, Perak Darul Ridzuan, Malaysia*
[3]*Chemical Engineering Department, Universiti Teknologi Petronas, 32610 Bandar Seri Iskandar, Perak Darul Ridzuan, Malaysia*
[4]*Adjunct Professors, Indian Institute of Technology, Kharagpur, India*

Correspondence should be addressed to Dzeti F. Mohshim; dzetifarhah@gmail.com and Hilmi Mukhtar; hilmi_mukhtar@utp.edu.my

Received 30 November 2018; Revised 28 February 2019; Accepted 17 March 2019; Published 2 May 2019

Academic Editor: Eric Guibal

Ionic liquid mixed matrix membranes (IL3Ms) were synthesized using polyethersulfone (PES) as the base polymer and silica-aluminophosphate (SAPO-34) as the dispersed particles, and their CO_2 permeation was investigated. Three of the most widely used models for gas separation—the Maxwell, Lewis–Nielson, and Maxwell–Wagner–Sillar (MWS) models—were then applied to the membranes. Large deviations were found between the model predictions and experimental data. FESEM images suggested that local agglomeration and disorientation of the SAPO-34 particles within the membrane afforded substantial changes in the morphology. The MWS model, which considers the shape factor, was modified to incorporate the volume fraction of the wetted dispersed phase and the ideal shape factor. A direct relationship was found between the filler concentration and the shape factor. The modified model was shown to produce absolute and relative errors of less than 3%. When validated against data from the literature, the deviation remained within 5%. The modified model can be used to estimate the gas permeance of an IL3M.

1. Introduction

Membranes, both polymeric and inorganic, have several specific advantages over conventional separation processes and are finding increasing applications in both gas and liquid separation. This has accelerated research in this area, particularly in the identification and development of new membrane materials. In gas separation, the major challenge is to synthesize membranes that can touch, if not cross, the Robeson plot [1] in terms of flux and selectivity or separation factor. Mixed matrix membranes (MMMs) are promising novel materials, and their high potential in both gas and liquid separation has already been recognized.

Transport of small gas molecules through a polymeric dense membrane occurs when random molecular motions are projected by the polymer matrix. The driving force in this process of sorption, diffusion, and permeation is the concentration gradient or partial pressure difference across the membrane [2, 3]. In sieving materials, gas transportation is driven by the difference in diffusion rates between permeating molecules of different shapes and sizes. More specifically, the rate of diffusion is determined by the gas penetrant and the sieving pore size [4]. Molecular sieving materials are known to offer high separation factors since their pore dimensions are similar to the dimensions of the gas molecules. Diffusion occurs when the molecules jump through a narrow opening between one sorption cavity and the next [5]. Adsorption and surface diffusion are further factors in gas permeation through small-pore-diameter membranes [6].

MMMs are heterogeneous membranes that generally constitute inorganic fillers dispersed within a polymer matrix, although the inclusion of organic or metal-organic

framework materials has also shown excellent potential [7]. In the ideal MMM morphology, a defect-free boundary is assumed between the dispersed particles and polymer interface [8]. The strong adhesion between the polymer and filler reduces the free volume in the polymer [9]—a process known as polymer rigidification [10]. In most cases, this rigidification [11] improves selectivity while reducing permeability [12].

With proper selection of the filler, many MMMs are excellent separation media for use in gas separation. However, there remains a need to improve both the flux and selectivity of MMMs. This can be achieved by appropriate manipulation of the membrane. In the proposed approach, an ionic liquid is incorporated into the membrane matrix. Ionic liquids are a large family of green solvents that demonstrate excellent solvent properties in addition to being nonvolatile and stable even at high temperatures. For membrane gas separation, many studies have investigated the use of ionic liquids in the form of supported liquid membranes (SLMs) and have yielded encouraging results [13–15]. Ionic liquids have also been polymerized to produce ionic liquid polymeric membranes (ILPMs) [16–18]. However, the permeation separation performance of these membranes is still lower than that of SLM and is yet to exceed the 2008 Robeson upper bound. A study mentioned by Ilyas et al. [19] has successfully synthesized supported ionic liquid membranes with 41 CO_2/CH_4 selectivity with no observation of ionic liquid leaching. It was a very good finding but it was limited to 10 bar, and the group has not focusing the effects of inorganic materials. Another work from Bhattacharya and Mandal [20], which was also not considering the effects of inorganic materials, has successfully tested their MMM at a maximum pressure of ~7 bar and found the membranes work better for H_2S/CH_4 separation. Based on these studies of using ionic liquid, it can be concluded that the ionic liquid can be the way forward of commercializing the membranes for gas separation purposes.

In this study, an ionic liquid was homogeneously distributed in the casting suspension and used to prepare an MMM comprising both fine adsorbent particles (SAPO-34) and an ionic liquid. The goal of this study was to achieve improvements in both flux and selectivity. The study also attempted to develop models suitable for predicting gas transportation in the membrane that considers the membrane's composition, characteristics, and morphology. A proper theoretical understanding of gas transportation in an MMM is required to support the design of research and development studies and to allow its implementation in industrial separation [21].

Gas transportation across MMMs has been a major focus of recent membrane research, mainly owing to their increasing use in gas-sweetening applications. Most existing theoretical models rely on old equations that were developed to address the quite different problem of estimating the electrical conductivity of a nonhomogeneous substance comprising a dispersed solid phase. By assuming that an analogy can be drawn with gas permeation, these conductivity models have been used to evaluate gas separation [22]. Similar electrical and thermal conductivity models have been applied to the analysis of MMMs [23].

Different models have used different approaches to predict the relative permeability of gases. Based on a review from Aroon et al. [8, 24], there are few permeation models used to predict effective permeability of a gaseous penetrant for mixed matrix membranes comprising porous particles. Another study from Hashemifard et al. [23] was also considering the models reviewed in [24] for their prediction of the relative permeability. In this study, the Maxwell, Lewis–Nielson, and Maxwell–Wagner–Sillar (MWS) models were used. However, these models cannot predict the permeability of a gas species through an MMM comprising a third component. One objective of the study was therefore to evaluate the existing models and to establish the adjustments needed to make them applicable for predicting gas transport across an IL3M. The MMM used in this study was prepared using polyethersulfone (PES), SAPO-34, and an ionic liquid. The analysis focused on the effect of the ionic liquid on the dispersion geometry of the SAPO-34 particles. This reflected our reported finding that incorporation of an ionic liquid triggers agglomeration of an inorganic filler within the membrane matrix [25].

2. Evaluation of Existing MMM Transport Models

Predicting the permeability of an MMM has proved a challenge. Interestingly, the theoretical models developed to address electrical conductivity in a nonhomogeneous medium are applicable to this entirely different problem, including the models proposed by Maxwell, Bruggeman, Pal, and Lewis–Nielson [8, 21, 23, 26, 27]. These models have received attention primarily because of their simplicity—the permeability of the MMM can be assumed to depend on those of the base polymer and the dispersed phase and the loading of the filler in terms of volume fraction [10]. The MWS model also incorporates the particle shape factor. Hashemifard et al. [15] and Nasir et al. [28] reviewed the applicability of the models at different particle loadings. Table 1 lists the available models and the parameters they require to estimate permeability.

The Maxwell model (equation (1) in Table 1) was first developed in 1873 to predict the permittivity of dielectric conduction through a heterogeneous medium [34]. The model involves a constitutive equation in which the heterogeneous medium is assumed to be an analogue of the membrane flux. This allows the model to be applied for gas transportation in an MMM. However, the Maxwell model fails when a high loading of filler in the MMM produces the maximum packing of the volume fraction. Furthermore, this model is not suitable for predicting permeation when parameters such as the shape, size distribution, and aggregation of the particles must be considered.

An alternative model was originally proposed to derive the elastic modulus of particulate composites. This is known as the Lewis–Nielson model and is given by equation (4) in Table 1 [32]. For random close packing of uniform spheres, ϕ_m is normally set at 0.64 [22]. When $\phi = \phi_m$, the permeability ratio $\lambda_{dm} \longrightarrow \infty$ as the relative permeability diverges.

Table 1: Theoretical models for mixed matrix membranes

Model	Equation	Equation number	Annotations	References
Maxwell	$P_r = (P/P_m) = [(2(1-\phi_d) + (1+2\phi_d)\lambda_{dm})/((2+\phi_d) + (1-\phi_d)\lambda_{dm})]$	(1)	P: permeability of penetrants	[29]
Bruggeman	$P_r^{1/3}[(\lambda_{dm}-1)/(\lambda_{dm}-P_r)] = (1-\phi_d)^{-1}$	(2)	P_r: relative permeability	[30]
Pal	$(P_r)^{1/3}[(\lambda_{dm}-1)/(\lambda_{dm}-P_m)] = (1-(\phi_d/\phi_m))^{-\phi_m}$	(3)	P_d: dispersed phase permeability	[22]
Lewis–Nielson	$P_r = (P/P_m) = [(1+(2((\lambda_{dm}-1)/(\lambda_{dm}+2)))\phi_d)/(1-((\lambda_{dm}-1)/(\lambda_{dm}+2))\phi_d\psi)]$	(4)	P_m: polymer matrix permeability ϕ_d: volume fraction of filler $\lambda_{dm} = (P_d/P_m)$	[31, 32]
	Where $\psi = 1 + ((1-\phi_d)/\phi_m^2)$	(5)		
Maxwell–Wagner–Sillar	$P_{eff} = P_m[(nP_d + (1-n)P_m - (1-n)\phi_d(P_m-P_d))/(nP_d + (1-n)P_m + n\phi(P_m-P_d))]$	(6)	ϕ_m: maximum volume fraction of filler n: shape factor	[33]

In this case, ϕ_m is very sensitive as it is affected by the shape, size distribution, and aggregation of the particles. However, the Lewis–Nielson model does not consider these parameters. As $\phi_m \longrightarrow 1$, the Lewis–Nielson model reduces to the Maxwell model.

The Pal model (equation (3) in Table 1) was developed for calculating the thermal conductivity of a composite particulate and has also been used to calculate permeability [35]. This model addresses the filler particle packing problem by applying a differential effective medium approach. The Pal model correctly predicts the behavior as $\phi \longrightarrow \phi_m$ by considering the effect of morphology on permeability through parameter ϕ_m. However, it involves an implicit relationship that must be solved numerically for the relative permeability, P_r.

Bouma et al. used the MWS model to predict the gas transportation characteristics of an MMM [33]. This model is given by equation (6) in Table 1, where n is the shape factor of the particle. Notably, the maximum and minimum values of the shape factor are used to derive the effective permeability of gas diffusion in an MMM, and these can be given by series or parallel models, respectively. However, no current model allows the effect of a third component (e.g., an ionic liquid) homogeneously distributed in the continuous membrane matrix to be considered when calculating the gas permeability of an IL3M. This study addressed the effect of adding an ionic liquid to an MMM and the optimization of the parameter affected by the ionic liquid in the theoretical calculation of CO_2 permeability.

3. Membrane Synthesis and Permeation Measurement

An MMM is a combination of polymer and molecular sieves. By combining the process characteristics of the polymer matrix and the superior transportation properties of the molecular sieve, MMMs combine the benefits of both materials [36]. In recent research, MMMs have been combined with ionic liquids to produce IL3Ms.

3.1. Synthesis of the Ionic Liquid Mixed Matrix Membranes. In this study, PES was chosen to provide the polymer support required for fabricating the enhanced MMM. This was the commercial Ultrason E 6020 P used in industrial processing and was purchased from BASF, Germany, in flake form. Commercial SAPO-34 with a kinetic diameter of 0.38 nm was purchased from ACS Material in powder form. Two ionic liquids of 99% purity were used: 1-ethyl-3-methylimidazolium bis(trifluoromethyl-sulfonyl)imide (emim [Tf_2N]) and 1-ethyl-3-methylimidazolium trifluoromethanesulfonate (emim[CF_3SO_3]). These were purchased from Sigma Aldrich and used without further purification. The IL3M synthesized using emim[Tf_2N] (IL3M-emim[Tf_2N]) was used for model correlation, while that synthesized using emim[CF_3SO_3] (IL3M-emim [CF_3SO_3]) was used for validation.

The PES flakes were dried overnight prior to use to remove any trapped moisture. The ionic liquid was mixed with the N-methyl-2-pyrrolidone (NMP) solvent, and the SAPO-34 particles were dispersed in the mixture. The PES was then dried and weighed, before being dissolved in the mixture. The solution was stirred continuously to ensure homogeneity and degassed to remove bubbles prior to casting. The cast membranes were dried in an oven at 160°C for 24 h. The details of the materials used, method of membrane preparation, and membrane characterization are presented in more detail in our recent publication [25]. For use as a benchmark, a PES-based polymeric membrane was synthesized. The IL3Ms were synthesized using a fixed ionic-liquid concentration of 20 wt.% and SAPO-34 filler concentrations of 10, 20, and 30 wt.%.

3.2. Membrane Morphology Characterization. Membrane morphology is critical for understanding transport mechanisms. This was characterized in the present study to clarify the effect of the added ionic liquid on the SAPO-34 orientation in the membrane matrix. Field emission scanning electron microscopy (FESEM, ZEIS SUPRA TM 55VP) was used for this characterization. Before scanning, the membranes were cut using liquid nitrogen to provide a smooth surface. Figure 1 shows the FESEM membrane sample of PES-SAPO-34 mixed matrix membrane with 10 wt.% ionic liquids. The average membrane thickness of all synthesized membranes is ~10 μm.

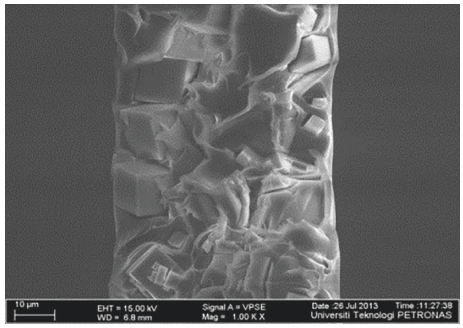

Figure 1: Sample of PES-SAPO-34 mixed matrix membranes with 10 wt.% ionic liquids.

3.3. Gas Separation Performance Analysis. Gas permeance analyses were conducted following the procedure reported in our previous study [25]. Gas permeation was then calculated from the time taken by the gas mixture to pass across the membrane at constant volume. This was recorded using a bubble flow meter, after a steady-state condition had been reached. The separation performance study was conducted at a pressure range of 10–30 bar. To ensure the reliability of the results, three membranes were fabricated using each composition, and all the fabricated membranes were tested using the same gas permeation method.

4. Present Model

Three of the models listed in Table 1 were selected for validation purposes: the Maxwell, Lewis–Nielson, and MWS models. Statistical analysis was performed to assess the level of agreement between the experimental data and the predictions made by the models. When deriving the gas permeance using the theoretical models, a defect-free PES membrane was assumed. The experimental data on CO_2 permeance are given in Table 2. The CO_2 permeance of SAPO-34 was taken from the literature [37]. Since the only data available on CO_2 permeance through an inorganic SAPO-34 membrane were obtained at a test pressure of 20 bar, the experimental data were also recorded at 20 bar. Two types of imidazolium-based ionic liquids were used to synthesize the IL3Ms. The gas permeation data for the IL3M-emim[Tf_2N] were used for model development.

The MWS model required the shape factor of the SAPO-34 particles to be specified. Based on [38], a value of $n = 0.33$ was used because SAPO-34 has a cubic form, as shown in the FESEM image in Figure 2. Figure 3 compares the relative permeance of CO_2 against SAPO-34 loading predicted by the above-mentioned three models with the experimentally determined values.

The absolute average error (AARE) was calculated using equation (1), and Table 3 summarizes the deviations between the models and the experimental data:

$$\mathrm{AARE}_i\,(\%) = \frac{100}{N}\sum_{i=1}^{N}\left|\frac{P_i^{\mathrm{cal}} - P_i^{\mathrm{exp}}}{P_i^{\mathrm{exp}}}\right|. \quad (1)$$

From Table 3, the relative permeability predicted by the existing models showed a major deviation from the experimental data; the AARE values were high (>50%), suggesting the need for model improvement and modification. Figure 4 shows FESEM images of the SAPO-34 orientation in the PES polymer matrix at different

Table 2: Experimental results for CO_2 permeation of PES membranes and IL3Ms at 20 bar.

SAPO-34 loadings (%)	Membranes	CO_2 permeance (GPU) (10^{-6} cm^3 (S.T.P)/ (s·cm^2·cmHg))	$P_r = P/P_m$	Reference
0	PES membrane	23.45	1	This study
10	IL3M1_20_10	352.43	15.02	
20	IL3M1_20_20	383.44	16.35	
30	IL3M1_20_30	408.41	17.42	
100	SAPO-34	1731.34	73.96	[37]

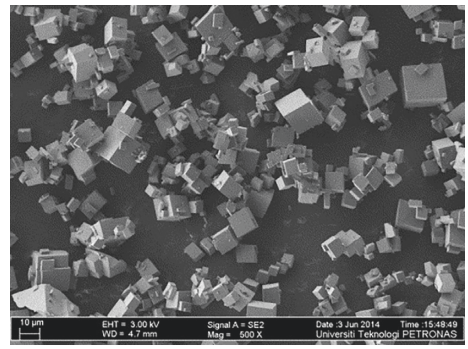

Figure 2: FESEM image of pure SAPO-34.

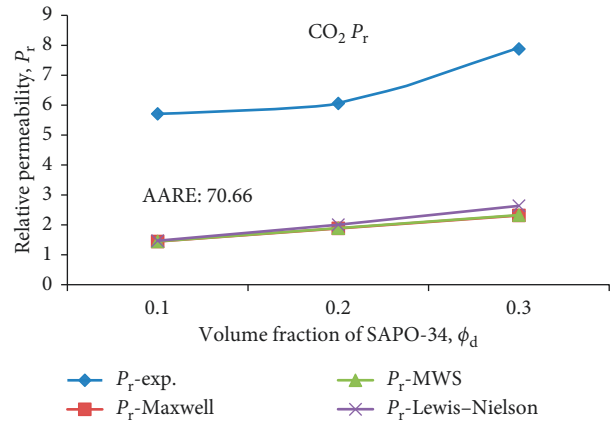

Figure 3: Relationships between experimental and theoretical relative permeability against SAPO-34 volume fraction at 20 bar.

Table 3: Deviation of model values from experimental data for CO_2 relative permeability at 20 bar pressure (data from Table 2).

Models	AARE
MWS	52.70
Maxwell	85.10
Lewis–Nielson	84.07

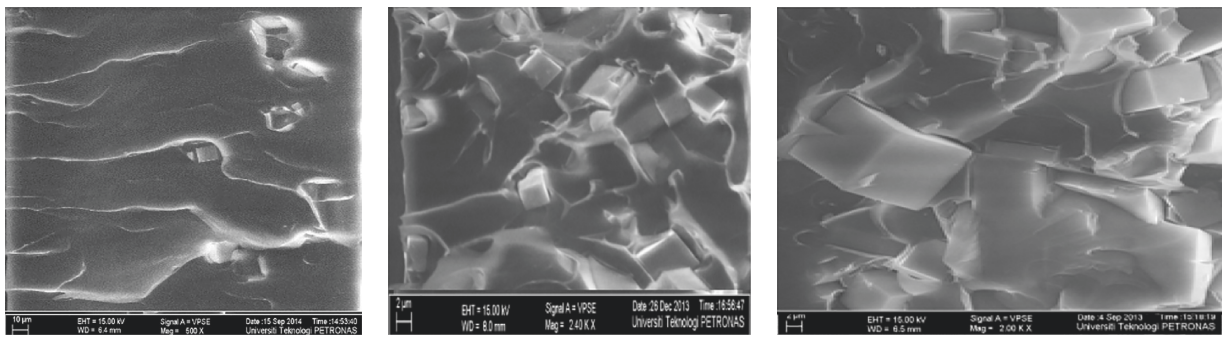

(a) (b) (c)

Figure 4: (a) 10 w/w%, (b) 20 w/w%, and (c) 30 w/w% SAPO-34 loading in ionic liquid mixed matrix membranes.

loadings. The FESEM analysis allowed the effective shape of the fillers to be determined as the loading was increased. The addition of ionic liquid caused the SAPO-34 to agglomerate, thereby changing the overall orientation of the inorganic filler. The analyses conducted using the theoretical models highlighted the importance of considering the morphology of the particles. As noted above, MWS is the only model that allows this. This model was therefore selected for modification, to bring it into line with the experimental data. A corrected parameter is needed to enable use of the model for accurate prediction of gas separation in an IL3M.

The FESEM cross sections revealed that the orientation of the SAPO-34 depended on the filler and the ionic liquid loading. The addition of ionic liquid changed the overall orientation of the SAPO-34 such that the resulting shape was no longer cubic, as shown in Figure 2. This resulted from the SAPO-34 particles agglomerating and combining with each other. This agglomeration became more pronounced as the SAPO-34 loading was increased. The FESEM results established that the shape factor is an important parameter in determining the P_r theoretical value since it may also favor enhancement of permeation via the hopping mechanism. As shown in Figure 4, the orientation of the filler within the membranes changed as the SAPO-34 loading in the membrane was increased. The SAPO-34 agglomerated locally. This became more pronounced as the loadings reached 20 and 30 w/w%, suggesting that the overall shape of the combined filler was also changing. To consider the shape factor, the MWS model required the optimization and improvement discussed in the following section.

5. Model Improvement and Optimization

To improve the MWS model, an additional parameter was incorporated. This modeled the effect that addition of the ionic liquid had on the orientation of the particle shapes. It was assumed that the addition of ionic liquid wetted the inorganic fillers, producing an undefined geometrical orientation of the fillers in the polymer matrix. Figure 5 shows these parameters.

The ionic liquid was assumed to wet the inorganic particles, making ϕ_d and n sensitive to their distribution,

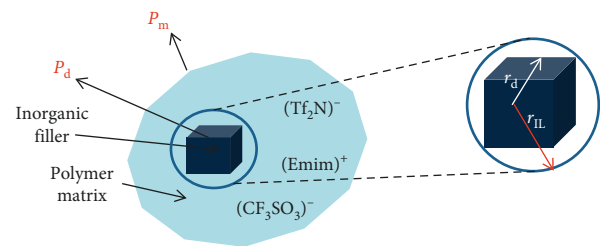

Figure 5: Schematic representation of ionic liquid mixed matrix membranes.

size, and orientation. The presence of ionic liquid also caused the SAPO-34 to become wetted, thereby increasing the volume fraction of the fillers. In practice, these parameters are difficult to determine directly via FESEM analysis. The model prediction can be made accurate if these parameters are fitted for each filler loading, as the morphology is a function of the filler loading. The MWS model developed in this study for use with an IL3M was modified to incorporate a corrected shape factor, n_i, and the volume fraction of the wetted dispersed phase, ϕ_w:

$$P_{eff} = P_m \left[\frac{n_i P_d + (1-n_i) P_m - (1-n_i)\phi_w (P_m - P_d)}{n_i P_d + (1-n_i) P_m + n_i \phi_w (P_m - P_d)} \right], \quad (2)$$

where n_i is the ideal shape factor (corrected shape factor) and ϕ_w is the wetted volume fraction of the dispersed phase through the IL3M. The volume fraction of the wetted dispersed phase, ϕ_w, was then redefined as follows:

$$\phi_w = \phi_d + \phi_{IL}, \quad (3)$$

where ϕ_{IL} is the ratio of the ionic liquid distance that has surrounded the particles as shown in Figure 5, determined as follows:

$$\phi_{IL} = \frac{r_{IL}}{r_d + r_{IL}}, \quad (4)$$

where $r_{IL}$is the radius of the ionic liquid surrounding the dispersed phase, r_d is the radius of the dispersed phase itself, and ϕ_{IL} is determined from the correlation between ϕ_w and ϕ_d obtained from the fitting analysis. If there is no wetting effect from the ionic liquid, ϕ_w will reduce to ϕ_d.

Physically, the ideal shape factor, n_i, is the shape factor of the SAPO-34 particles after incorporation of ionic liquid since the ionic liquid affects the SAPO-34 orientation in the polymer matrix. This is defined as follows:

$$n_i = n_o \frac{\phi_w}{\phi_m}, \quad (5)$$

where n_o is the optimized shape factor from the fitting exercise and ϕ_m is the maximum packing volume fraction of the inorganic filler ($\phi_m = 0.64$). If $\phi_w = \phi_m$, n_i is reduced to n_o. Sikander (2015) obtained an expression similar to equation (5) when optimizing the shape factor [39]. Any intermediate point value should therefore be directly obtainable from equation (5).

5.1. Determination of Volume Fraction of Wetted Dispersed Phase ϕ_w. The objective of this approach is to optimize the volume fraction of the wetted dispersed phase and to find the correlation between ϕ_w and ϕ_d, as given by equation (3). The optimization procedures conducted against the experimental data were used to generate the ϕ_w values shown in Table 4. These values demonstrate that the incorporation of ionic liquid was sufficient to wet the SAPO-34, eventually increasing the volume fraction of the wetted dispersed phase, ϕ_w.

5.2. Determination of Ideal Shape Factor, n_i. The ideal shape factor, n_i, used in equation (5) was determined via optimization analysis. Figure 6 shows the optimization curve obtained by applying the optimization procedure to the original MWS model against the experimental data. The evaluation of relative CO_2 permeability was repeated using the optimized shape factor $n_o = 0.020$, and a lower AARE (<25%) was returned. This analysis confirmed that the n parameter can be used to improve the predictions made by the model if the optimized values are known. Even the use of a single optimized value of n_o improved the MWS model predictions, and the accuracy could be further improved if the shape factor could be fitted at a specific SAPO-34 loading. This reflects the fact that the membrane morphology is a function of the distribution and aggregation of the particles.

If the shape factor at a specific SAPO-34 loading is known, the gas relative permeability at any operating pressure can be predicted since the shape factor is independent of pressure. The n_i factor was introduced to reflect the orientation and distribution of the particles. Optimization of the n_i value produced the results shown in Table 5.

As equation (5) shows, the ideal shape factor depends on the value of ϕ_w. The n_i value is therefore expected to increase in line with the SAPO-34 loadings.

5.3. Determination of the Corrected Dispersed Phase Permeability, P_d. The actual dispersed phase permeability, P_d, of CO_2 across SAPO-34 is critical to determine $P_{r(eff)}$ in equation (6) in Table 1. Since the P_d value given in [37] was for SAPO-34 loading at 20-bar pressure, P_d (CO_2) = 1731.4 GPU was used in the present study to evaluate the theoretical performance only at this pressure. In addition, the effect of pressure on relative permeability was investigated, and the P_d values for CO_2 at the other testing pressures needed to be optimized accordingly.

The fitting and optimization for P_d was performed using an indirect method. The least squares method was applied to the variable parameter values to reduce the predicted errors from the model. The corrected P_d was obtained when the least error resulted. Since the fitting method worked for 10 wt.% of SAPO-34, it was also used to determine the corrected P_d at 20 wt.% and 30 wt.%. Table 6 summarizes the fitted CO_2 P_d values for all SAPO-34 loadings at pressures of 10, 15, 25, and 30 bar. The P_d value at 20 bar was as stated and maintained accordingly.

As can be seen from Table 6, the optimized CO_2 P_d values decreased with increasing pressure. This might be due to the concentration polarization of the intrinsic SAPO-34 inorganic membrane. Van de Graaf et al. reported that CH_4 became enriched at the support pores, eventually depleting the driving force of the quickly permeating gas. The depletion of CO_2 at increased pressures was also attributed to

Table 4: Fitted ϕ_w values against SAPO-34 volume fraction of IL3M-emim[Tf_2N].

SAPO-34 loading, ϕ_d (wt.%)	ϕ_d	Volume fraction of wetted dispersed phase, ϕ_w
10	0.1340	0.2817
20	0.2363	0.3538
30	0.3170	0.4133

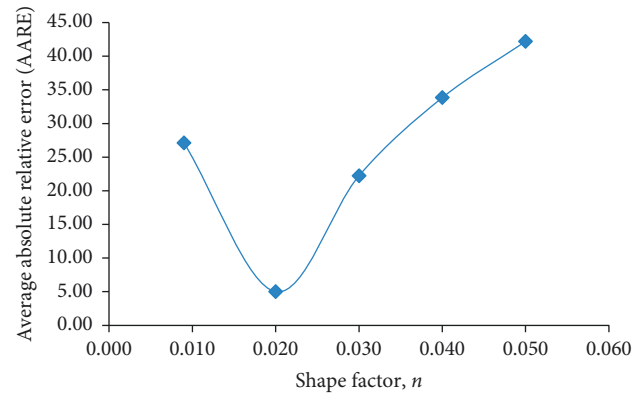

Figure 6: Optimization curve of shape factor, n, through a shape factor data fitting.

Table 5: Values of ideal shape factor at different SAPO-34 loadings of IL3M-emim[Tf_2N].

ϕ_d	Optimized shape factor, n_o	Ideal shape factor, n_i
0.134021		0.009
0.236364	0.020	0.016
0.317073		0.021

Table 6: Optimized P_d for CO_2.

Pressure (bar)	ϕ_w	CO_2 optimized P_d
10		2624.68
15		2000.07
20	0.2817	1731.40
25		1420.03
30		1419.86
10		4460.16
15		2382.84
20	0.3538	1731.40
25		1543.42
30		1289.37
10		5799.36
15		2462.93
20	0.4133	1731.40
25		1435.59
30		1341.04

the high diffusion resistance caused by the enrichment of CH_4 at the support [40]. Avila et al. reported that the concentration polarization became more pronounced at a pressure of 5.8 MPa, owing to the growth of separation layers at the tubular support [41].

5.4. Results of Model Modification. After applying the above modifications, the theoretical predictions of CO_2 relative permeability ($P_{r(eff)}$) for the PES-SAPO-34 IL3Ms were calculated using equation (2). Table 7 shows the relationship between P_r-experimental and P_r-calculated for CO_2. The AARE between the experimental and calculated P_r values was less than 2%.

For clarity, the relationship between P_r-experimental and P_r-calculated is plotted in Figure 7. The results confirm that the modified model successfully predicted the CO_2 relative permeability of the IL3M.

6. Model Validation

6.1. Validation Using Different Data. As noted above, IL3M-emim[CF_3SO_3] was used for validation. The value of the dispersed phase permeability, P_d, was that used in the previous section. However, the volume fraction of the wetted dispersed phase, ϕ_w, and the ideal shape factor, n_i, needed correction since a different ionic liquid was used. To determine these values, the correlations obtained from equations (3) and (5) were applied to ϕ_w and n_i, respectively. Table 8 shows the ϕ_w and n_i values for the IL3M-emim [CF_3SO_3].

The CO_2 relative permeability ($P_{r(eff)}$) of the PES-SAPO-34-emim[CF_3SO_3] IL3M was predicted theoretically using equation (12). Table 9 shows the relationship between the P_r-experimental and P_r-calculated values. The AARE between the experimental and calculated P_r values was less than 3%. The approach was shown to achieve better agreement between the experimental and calculated values of $P_{r(eff)}$. The experimental and calculated values of P_r are shown in Figure 8, with $R^2 = 0.95$.

Table 7: P_r-calculated and P_r-experimental for CO_2 of IL3M-emim [Tf_2N] using the modified MWS model.

Pressure (bar)	ϕ_w	n_i	P_m	P_d	P_r-Cal	P_r-Exp	AARE
10			25.43	2624.68	18.4604	19.16	
15			24.48	2000.07	16.0317	15.53	
20	0.2817	0.009	23.45	1731.40	15.0276	15.03	1.98
25			23.21	1420.03	13.2667	13.01	
30			20.03	1419.86	14.6349	14.49	
10			25.43	4460.16	23.3738	23.56	
15			24.48	2382.84	18.2940	18.92	
20	0.3538	0.016	23.45	1731.40	15.8591	16.35	2.11
25			23.21	1543.42	14.9595	15.19	
30			20.03	1289.37	14.6816	14.98	
10			25.43	5799.36	25.7782	26.09	
15			24.48	2462.93	19.5223	20.05	
20	0.4133	0.021	23.45	1731.40	16.8919	17.41	1.76
25			23.21	1435.59	15.3973	15.40	
30			20.03	1341.04	16.0625	16.39	

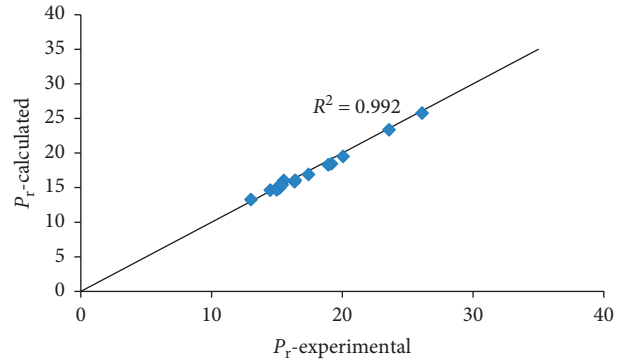

Figure 7: Experimental and calculated values of CO_2 relative permeability for emim[Tf2N]

Table 8: Modified parameters for the SAPO-34 volume fraction of IL3M-emim[CF_3SO_3].

ϕ_d	Wetted volume fraction of dispersed phase, ϕ_w	Ideal shape factor, n_i
0.1340	0.2710	0.010
0.2363	0.3507	0.016
0.3170	0.4124	0.021

6.2. Validation Using Data from the Literature. In this section, we review data from the literature on membrane fabrication incorporating ionic liquids. Hudiono et al. investigated CO_2/CH_4 separation using MMMs comprising a styrene-based polymer, SAPO-34 as the zeolite filler, and emim[Tf_2N] as the ionic liquid [17]. The CO_2 permeability reported in that study is shown in Table 10. The study confirmed that the incorporation of a sufficient volume of ionic liquid into the styrene-based-SAPO-34 MMM increased CO_2 permeability and selectivity. They concluded that the addition of ionic liquid had wetted the surface of the SAPO-34, making it compatible with the styrene-based poly(RTIL). The high CO_2 diffusivity of the emim[Tf_2N] produced an overall enhancement of gas permeability.

Table 9: P_r-calculated and P_r-experimental values for CO_2 of IL3M-emim[CF_3SO_3] using the modified MWS model.

Pressure	ϕ_w	n_i	P_m	P_d	P_r-Cal	P_r-Exp	AARE
10			25.43	2624.68	16.8781	18.75	
15			24.48	2000.07	14.7746	14.96	
20	0.2710	0.010	23.45	1731.40	13.8954	13.44	4.27
25			23.21	1420.03	12.3401	12.51	
30			20.03	1419.86	13.5501	14.32	
10			25.43	4460.16	22.5853	21.60	
15			24.48	2382.84	17.7870	16.94	
20	0.3507	0.016	23.45	1731.40	15.4661	16.09	3.71
25			23.21	1543.42	14.6051	14.08	
30			20.03	1289.37	14.3387	14.15	
10			25.43	5799.36	25.4659	25.68	
15			24.48	2462.93	19.3378	19.20	
20	0.4124	0.021	23.45	1731.40	16.7514	16.75	2.04
25			23.21	1435.59	15.2791	14.29	
30			20.03	1341.04	15.9346	16.22	

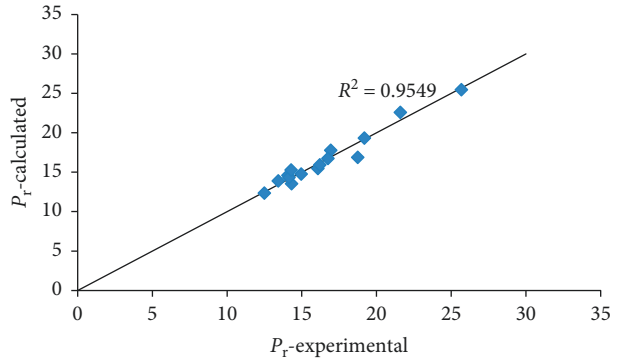

Figure 8: Experimental and calculated values of CO_2 relative permeability for emim[CF_3SO_3].

Table 10: CO_2 permeability of three-component MMMs [17].

Membrane	SAPO-34 loading (wt.%)	Emim[Tf_2N] loading (wt.%)	CO_2 permeability, P_m (barrer)	CO_2 relative permeability, P_r
M1	—	—	9.2	1
M2	10	18	72.1	7.84
M3	20	32	181.7	19.75
M4	40	36	564.4	61.35

Table 11: Validation of model parameters for CO_2 relative permeability using data from the literature.

ϕ_w	P_m	P_d	Ideal shape factor, n_i	CO_2 relative permeability, P_r Calculated	CO_2 relative permeability, P_r Experimental	AARE
0.10	9.2	1731.40	0.009	8.66	7.84	
0.45	9.2	1731.40	0.016	20.15	19.75	4.83
0.71	9.2	1731.40	0.021	60.11	61.34	

This study suggested that the presence of ionic liquid changed the orientation of the SAPO-34. The ideal shape factor, n_i, was therefore introduced by incorporating the ionic liquid concentration into the model. The SAPO-34 fillers were also believed to have been wetted by the RTIL, and ϕ_w was also calculated using equation (3). The ideal shape factor, n_i, was calculated using equation (5). The CO_2 relative permeability was recalculated using equation (12), which incorporated both ϕ_w and n_i. The calculated data are shown in Table 11, and the relationship between the experimental and theoretical data is presented in Figure 9.

As can be seen from Table 11, the AARE fell below 5% when the MWS model was modified by incorporating ϕ_w and n_i.

7. Conclusions

Three of the most widely used models for estimating the permeability of a gas through an MMM were applied to

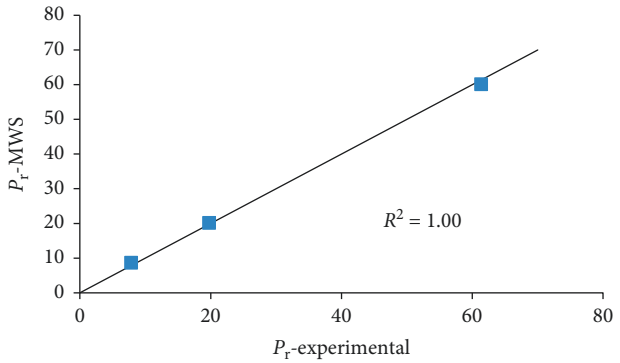

FIGURE 9: CO_2 relative permeability comparison of experimental data [17] and theoretical values.

membranes modified by adding an ionic liquid. All three models showed high rates of error. The effective shape factor was found to be a critical parameter in the MWS model. The addition of ionic liquid had produced local agglomeration of SAPO-34 within the membrane matrix, thereby changing the overall orientation of the filler. Therefore, the shape factor was modified to include both the ionic liquid and filler loading effects. The ideal shape factor, n_i, and volume fraction of wetted dispersed phase, ϕ_w, were determined. Calculating relative permeance using a modified MWS model incorporating ϕ_w and n_i showed better agreement between the experimental and predicted values. The modified model was validated against a different set of experimental data and against values reported in the literature. Both showed good agreement between the predicted and experimental values, with an AARE of less than 5%. Our results confirm that the modified MWS model can be used to predict the performance of IL3Ms.

Data Availability

Previously reported CO_2 and CH_4 permeability data were used to support this study and are available at https://doi.org/10.1016/j.seppur.2014.08.019. These prior studies (and datasets) are cited at relevant places within the text as reference [22].

Additional Points

(i) CO_2 permeation prediction was successfully modified through the Maxwell–Wagner–Sillar model. (ii) The effects of ionic liquid loading were embedded in the modified model. (iii) The AARE% between the experimental and model values is less than 5.

Conflicts of Interest

The authors declare that they have no conflicts of interest.

Acknowledgments

The authors would like to acknowledge the fund provided by the Ministry of Education (MOE), Malaysia (ERGS-0153AB-C67), and the assistance and support provided by Universiti Teknologi Petronas.

References

[1] L. M. Robeson, "The upper bound revisited," *Journal of Membrane Science*, vol. 320, no. 1-2, pp. 390–400, 2008.

[2] N. P. Cheremisinoff, *Handbook of Polymer Science and Technology*, CRC Press, Vol. 4, Boca Raton, FL, USA, 1989.

[3] H. A. Mannan, H. Mukhtar, T. Murugesan, R. Nasir, D. F. Mohshim, and A. Mushtaq, "Recent applications of polymer blends in gas separation membranes," *Chemical Engineering & Technology*, vol. 36, no. 11, pp. 1838–1846, 2013.

[4] P. S. Singh, T. Selvam, S. Reuß, A. Avhale, S. Lopez-Orozco, and W. Schwieger, "Nanocrystalline zeolite tetraethylammonium-beta membrane for preferential sorption and transport of CO_2 over N_2," *Chemical Engineering & Technology*, vol. 36, no. 7, pp. 1209–1216, 2013.

[5] R. Nasir, H. Mukhtar, Z. Man, and D. F. Mohshim, "Material advancements in fabrication of mixed-matrix membranes," *Chemical Engineering & Technology*, vol. 36, no. 5, pp. 717–727, 2013.

[6] R. W. Baker, *Membrane Technology and Applications*, Wiley, Hoboken, NJ, USA, 2012.

[7] G. Dong, H. Li, and V. Chen, "Challenges and opportunities for mixed-matrix membranes for gas separation," *Journal of Materials Chemistry A*, vol. 1, no. 15, pp. 4610–4630, 2013.

[8] H. Vinh-Thang and S. Kaliaguine, "Predictive models for mixed-matrix membrane performance: a review," *Chemical Reviews*, vol. 113, no. 7, pp. 4980–5028, 2013/07/10 2013.

[9] R. Mahajan, R. Burns, M. Schaeffer, and W. J. Koros, "Challenges in forming successful mixed matrix membranes with rigid polymeric materials," *Journal of Applied Polymer Science*, vol. 86, no. 4, pp. 881–890, 2002.

[10] Z. Huang, Y. Li, R. Wen, M. May Teoh, and S. Kulprathipanja, "Enhanced gas separation properties by using nanostructured PES-Zeolite 4A mixed matrix membranes," *Journal of Applied Polymer Science*, vol. 101, no. 6, pp. 3800–3805, 2006.

[11] T.-S. Chung, L. Y. Jiang, Y. Li, and S. Kulprathipanja, "Mixed matrix membranes (MMMs) comprising organic polymers with dispersed inorganic fillers for gas separation," *Progress in Polymer Science*, vol. 32, no. 4, pp. 483–507, 2007.

[12] S. Kulprathipanja, "Mixed matrix membrane development," *Membrane Technology*, vol. 2002, no. 4, pp. 9–12, 2002.

[13] G. Zarca, I. Ortiz, and A. Urtiaga, "Facilitated-transport supported ionic liquid membranes for the simultaneous recovery of hydrogen and carbon monoxide from nitrogen-enriched gas mixtures," *Chemical Engineering Research and Design*, vol. 92, no. 4, pp. 764–768, 2014.

[14] P. Jindaratsamee, A. Ito, S. Komuro, and Y. Shimoyama, "Separation of CO_2 from the CO_2/N_2 mixed gas through ionic liquid membranes at the high feed concentration," *Journal of Membrane Science*, vol. 423-424, pp. 27–32, 2012.

[15] S. A. Hashemifard, A. F. Ismail, and T. Matsuura, "A new theoretical gas permeability model using resistance modeling for mixed matrix membrane systems," *Journal of Membrane Science*, vol. 350, no. 1-2, pp. 259–268, 2010.

[16] L. Hao, P. Li, T. Yang, and T.-S. Chung, "Room temperature ionic liquid/ZIF-8 mixed-matrix membranes for natural gas sweetening and post-combustion CO_2 capture," *Journal of Membrane Science*, vol. 436, pp. 221–231, 2013.

[17] Y. C. Hudiono, T. K. Carlisle, A. L. LaFrate, D. L. Gin, and R. D. Noble, "Novel mixed matrix membranes based on

polymerizable room-temperature ionic liquids and SAPO-34 particles to improve CO_2 separation," *Journal of Membrane Science*, vol. 370, no. 1-2, pp. 141–148, 2011.

[18] P. Li, K. P. Pramoda, and T.-S. Chung, "CO_2 Separation from flue gas using polyvinyl-(room temperature ionic liquid)-room temperature ionic liquid composite membranes," *Industrial & Engineering Chemistry Research*, vol. 50, no. 15, pp. 9344–9353, 2011.

[19] A. Ilyas, N. Muhammad, M. A. Gilani, K. Ayub, I. F. J. Vankelecom, and A. L. Khan, "Supported protic ionic liquid membrane based on 3-(trimethoxysilyl)propan-1-aminium acetate for the highly selective separation of CO_2," *Journal of Membrane Science*, vol. 543, pp. 301–309, 2017.

[20] M. Bhattacharya and M. K. Mandal, "Synthesis and characterization of ionic liquid based mixed matrix membrane for acid gas separation," *Journal of Cleaner Production*, vol. 156, pp. 174–183, 2017.

[21] B. Shimekit, H. Mukhtar, and T. Murugesan, "Prediction of the relative permeability of gases in mixed matrix membranes," *Journal of Membrane Science*, vol. 373, no. 1-2, pp. 152–159, 2011.

[22] R. Pal, "Permeation models for mixed matrix membranes," *Journal of colloid and interface science*, vol. 317, no. 1, pp. 191–198, 2008.

[23] S. A. Hashemifard, A. F. Ismail, and T. Matsuura, "Prediction of gas permeability in mixed matrix membranes using theoretical models," *Journal of Membrane Science*, vol. 347, no. 1-2, pp. 53–61, 2010.

[24] M. A. Aroon, A. F. Ismail, T. Matsuura, and M. M. Montazer-Rahmati, "Performance studies of mixed matrix membranes for gas separation: a review," *Separation and Purification Technology*, vol. 75, no. 3, pp. 229–242, 2010.

[25] D. F. Mohshim, H. Mukhtar, and Z. Man, "The effect of incorporating ionic liquid into polyethersulfone-SAPO34 based mixed matrix membrane on CO_2 gas separation performance," *Separation and Purification Technology*, vol. 135, pp. 252–258, 2014.

[26] S. A. Hashemifard, A. F. Ismail, and T. Matsuura, "A new theoretical gas permeability model using resistance modeling for mixed matrix membrane systems," *Journal of Membrane Science*, vol. 350, no. 1-2, pp. 259–268, 2010.

[27] E. Gonzo, M. Parentis, and J. Gottifredi, "Estimating models for predicting effective permeability of mixed matrix membranes," *Journal of Membrane Science*, vol. 277, no. 1-2, pp. 46–54, 2006.

[28] R. Nasir, H. Mukhtar, and Z. Man, "Prediction of gas transport across amine mixed matrix membranes with ideal morphologies based on the Maxwell model," *RSC Advances*, vol. 6, no. 36, pp. 30130–30138, 2016.

[29] J. C. Maxwell, *Electricity and Magnetism*, Dover, Vol. 2, Downers Grove, IL, USA, 1954.

[30] D. A. G. Bruggeman, "Berechnung verschiedener physikalischer konstanten von heterogenen substanzen. I. Dielektrizitätskonstanten und leitfähigkeiten der mischkörper aus isotropen substanzen," *Annalen der Physik*, vol. 416, no. 7, pp. 636–664, 1935.

[31] T. B. Lewis and L. E. Nielsen, "Dynamic mechanical properties of particulate-filled composites," *Journal of Applied Polymer Science*, vol. 14, no. 6, pp. 1449–1471, 1970.

[32] L. E. Nielsen, "Thermal conductivity of particulate-filled polymers," *Journal of applied polymer science*, vol. 17, no. 12, pp. 3819-3820, 1973.

[33] R. H. B. Bouma, A. Checchetti, G. Chidichimo, and E. Drioli, "Permeation through a heterogeneous membrane: the effect of the dispersed phase," *Journal of Membrane Science*, vol. 128, no. 2, pp. 141–149, 1997.

[34] J. C. Maxwell, *A Treatise on Electricity and Magnetism*, Dover Publication, New York, NY, USA, 3rd edition, 1854.

[35] R. Pal, "New models for thermal conductivity of particulate composites," *Journal of Reinforced Plastics and Composites*, vol. 26, no. 7, pp. 643–651, 2007.

[36] D. F. Mohshim, H. b. Mukhtar, Z. Man, and R. Nasir, "Latest development on membrane fabrication for natural gas purification: a review," *Journal of Engineering*, vol. 2013, Article ID 101746, 7 pages, 2013.

[37] M. A. Carreon, S. Li, J. L. Falconer, and R. D. Noble, "Alumina-supported SAPO-34 membranes for CO_2/CH_4 separation," *Journal of the American Chemical Society*, vol. 130, no. 16, pp. 5412-5413, 2008.

[38] G. C. J. Bart and K. Hanjalić, "Estimation of shape factor for transient conduction," *International Journal of Refrigeration*, vol. 26, no. 3, pp. 360–367, 2003.

[39] S. Rafiq, A. Maulud, Z. Man et al., "Modelling in mixed matrix membranes for gas separation," *Canadian Journal of Chemical Engineering*, vol. 93, no. 1, pp. 88–95, 2015.

[40] J. M. van de Graaf, F. Kapteijn, and J. A. Moulijn, "Methodological and operational aspects of permeation measurements on silicalite-1 membranes," *Journal of Membrane Science*, vol. 144, no. 1-2, pp. 87–104, 1998.

[41] A. M. Avila, H. H. Funke, Y. Zhang, J. L. Falconer, and R. D. Noble, "Concentration polarization in SAPO-34 membranes at high pressures," *Journal of Membrane Science*, vol. 335, no. 1-2, pp. 32–36, 2009.